Electrical stress effect on Josephson tunneling through ultrathin AlO_x barrier in Nb/Al/AlO_x/Nb junctions

Sergey K. Tolpygo[1,2,3,a)] and Denis Amparo[2,b)]
[1]*HYPRES, Inc., 175 Clearbrook Road, Elmsford, New York 10523, USA*
[2]*Department of Physics and Astronomy, Stony Brook University, Stony Brook, New York 11794-3800, USA*
[3]*Department of Electrical and Computer Engineering, Stony Brook University, Stony Brook, New York 11794-2350, USA*

(Received 29 May 2008; accepted 11 July 2008; published online 19 September 2008)

The effect of dc electrical stress and breakdown on Josephson and quasiparticle tunneling in Nb/Al/AlO_x/Nb junctions with ultrathin AlO_x barriers typical for applications in superconductor digital electronics has been investigated. The junctions' conductance at room temperature and current-voltage (*I-V*) characteristics at 4.2 K have been measured after the consecutive stressing of the tunnel barrier at room temperature. Electrical stress was applied using current ramps with increasing amplitude ranging from 0 to $\sim 1000 I_c$ corresponding to voltages across the barrier up to ~ 0.65 V, where I_c is the Josephson critical current. A very soft breakdown has been observed with polarity-dependent breakdown current (voltage). As the stressing progresses, a dramatic increase in subgap conductance of the junctions, the appearance of subharmonic current steps, and a gradual increase in both the critical and the excess currents as well as a decrease in the normal-state resistance have been observed. The observed changes in superconducting tunneling suggest a model in which a progressively increasing number of defects and associated additional conduction channels [superconducting quantum point contacts (SQPCs)] are induced by electric field in the tunnel barrier. By comparing the *I-V* characteristics of these conduction channels with the nonstationary theory of current transport in SQPCs based on multiple Andreev reflections by Averin and Bardas, the typical transparency D of the induced SQPCs was estimated as $D \sim 0.7$. The number of induced SQPCs was found to grow with voltage across the barrier as $\sinh(V/V_0)$ with $V_0 = 0.045$ V, in good agreement with the proposed model of defect formation by ion electromigration. The observed polarity dependence of the breakdown current (voltage) is also consistent with the model. Based on the observed magnitude of breakdown currents, electric breakdown of AlO_x barrier during plasma processing was considered to be an unlikely cause of fabrication-induced, circuit pattern-dependent nonuniformities of Josephson junctions' critical currents in superconductor integrated circuits. © *2008 American Institute of Physics*. [DOI: 10.1063/1.2977725]

I. INTRODUCTION

Aluminum oxide (AlO_x) is widely used as a barrier material in various applications involving tunnel junctions. It was also considered as a potential gate oxide in advanced memory devices and metal-oxide-semiconductor (MOS) transistors. Dielectric reliability issues such as oxide barrier stability, leakage currents, and electric breakdown are very important for electronic applications, especially for magnetic tunnel junctions (MTJs) used for magnetic random access memories and superconducting tunnel junctions (STJs) used for superconductor digital circuits requiring ultrathin (~ 1 nm) tunnel barriers. The physics of dielectric breakdown in ultrathin barriers is of great interest in its own right. Oxide breakdowns are usually classified into two modes: intrinsic and extrinsic. Although the difference is somewhat blurry, extrinsic breakdowns are those caused by defects introduced or created during oxide growth, whereas intrinsic ones are the property of a perfect dielectric. In relatively thick oxide layers such as those used as gate dielectric in MOS transistors, electric breakdown usually proceeds by the accumulation of defects (traps) inside the dielectric until a percolation pass is formed, at which point the resistivity suddenly decreases from a very high value to a very low value, and a hard breakdown occurs.[1,2] In thinner oxide layers the breakdown often has a soft character which is characterized by small gradual changes in resistance.[3,4] The thickness of ultrathin tunnel barriers used in superconductor electronics is a couple of oxide monolayers, only a few interatomic distances. Therefore, any defects formed in the oxide as a result of electrical stress (e.g., displaced ions, oxygen vacancies, etc.) should create additional conduction channels with significantly increased transmission probability and consequently dramatically alter the quasiparticle and Cooper-pair tunneling. In other words, the percolation path forming at breakdown may consist of just a single defect (trap) and hence the breakdown may be very soft.

There have been several publications on the reliability and breakdown of aluminum oxide layers with thicknesses above ~ 3 nm as a new gate oxide and ~ 1 nm in MTJs.[5–9] The existence of both intrinsic and extrinsic breakdown modes was suggested.[7] The intrinsic mode was associated with a hard breakdown, and was suggested to be related to

a)Electronic mail: stolpygo@hypres.com.
b)Electronic mail: denis.amparo@sunysb.edu.

the chemical bond breaking in applied electric field.[10–12] The extrinsic mode was associated with a soft, gradual breakdown. It was suggested to be related to pre-existing pinholes in the barrier which grow in area as breakdown progresses due to Joule heating and/or electric field effect.[7]

Superconductor-insulator-superconductor (SIS) junctions offer unique opportunities in studying breakdown mechanisms in ultrathin oxides because both the quasiparticle and Josephson tunneling in STJs are extremely sensitive to the barrier properties and boundary conditions at the metal-oxide interfaces. In contrast to MTJs, pre-existing pinholes in SIS junctions are easily identifiable because they carry supercurrent thus creating nonuniform Josephson current distribution and dramatically increasing subgap conductance. Whereas a microshort in MTJs was associated with a junction having the resistance-area product RA of $\sim 0.8\ \Omega\ \mu m^2$, and no tunneling magnetoresistance,[7] STJs with even lower values of RA product exist and display interesting Josephson tunneling properties.[13–15]

Superconductor digital electronics utilizing SIS junctions has a potential for subterahertz clock frequencies and ultralow power dissipation for digital signal processing, high-performance communications, and computing.[16] Recently, complex superconducting circuits based on rapid single flux quantum (RSFQ) logic such as analog-to-digital converters and digital rf receivers containing thousands of logic gates with clock frequencies ~30 GHz have been demonstrated, operating not only in liquid He but also on commercial closed-cycle cryocoolers.[17] Increasing the clock frequencies of superconductor integrated circuits to ~100 GHz would require employing high-J_c junctions with RA products below $\sim 1\ \Omega\ \mu m^2$, perhaps the thinnest tunnel barriers among all known devices.[18,19]

Dielectric reliability may not appear to be important for superconducting digital circuits because they operate at very low temperatures and at very low voltages (~1 mV). Its significance however arises from the possibility that tunnel barrier degradation may occur during integrated circuit fabrication. For instance, the current state of the art in RSFQ circuits has been plagued by limited circuit yield brought about to a large extent by fabrication-induced variations on the Josephson critical current (I_c) of the tunnel junctions.[18,20] These variations may be related to dielectric barrier degradation and electrical breakdown. It has been observed, for example, that the I_c of Josephson tunnel junctions may depend on how the junction is wired to other circuit elements, and in particular, at which step in the fabrication process does the junction make electrical contact with the circuit's ground plane.[20] For series arrays of nominally identical tunnel junctions, it was frequently observed that the Josephson critical current of a few junctions (usually of the first and the last junction in the array) is significantly larger than for the rest of the junctions. This cannot be simply explained by a variation in the area of that one junction coming from the lithography and etch processes of junction definition. Neither can it be explained by a random fluctuation in the tunnel barrier transparency in that particular junction, considering that the effect reproduces in different arrays and the junctions in the array are just ~10 μm apart. Instead, it was suggested that the above phenomena are brought about by electrical currents flowing through the tunnel barriers, a result of plasma processing steps which follows the SIS trilayer deposition. Recent experiments involving tunnel junctions protected from plasma process-induced electric stress by current-limiting resistors support this suggestion.[21]

Surprisingly, there has been almost no research on the reliability of ultrathin AlO_x barriers in STJs, except for early works on $Al/AlO_x/Pb$ junctions which studied the effects of electric annealing on the barrier thickness, height, and asymmetry of AlO_x barriers formed by plasma oxidation.[22] These junctions, however, have no practical application, and the changes in superconducting and Josephson properties were not studied.

In this work, the effect of applied dc electrical stress on quasiparticle and Josephson tunneling in $Nb/Al/AlO_x/Nb$ junctions was investigated. The study focused on this type of junctions because of their dominant use in superconductor digital and analog electronics.

II. FABRICATION

The $Nb/Al/AlO_x/Nb$ junctions used in this study were fabricated at HYPRES, Inc. using an 11-level process for superconductor integrated circuits.[18,23] The fabrication was performed on 150 mm Si wafers. The process is based on *in situ* $Nb/Al/AlO_x/Nb$ trilayer deposition.[24] Specifically, Nb/Al bilayer (150 and 8 nm, respectively) deposition is followed by AlO_x formation by room temperature oxidation of Al. The AlO_x layer is then topped off by the deposition of the Nb counterelectrode (50 nm). All metal layers are deposited by dc magnetron sputtering in a cryopumped vacuum system with a base pressure of 1×10^{-9} Torr. Two Josephson critical current densities, J_c (1 and 4.5 kA/cm^2), were targeted, obtained by Al oxidation for 15 min at oxygen pressures of 170 and 18 mTorr, respectively. After the counterelectrode etch process that defines the junctions, their interior was sealed along the perimeter and sidewalls by an anodization layer composed of Al_2O_3 and Nb_2O_5 in order to protect the barrier from reacting with process chemicals used in subsequent fabrication steps.

Circular *JJ*'s with design radii of 2.00 μm ($A=12.6\ \mu m^2$) and 0.95 μm ($A=2.8\ \mu m^2$) for wafers with $J_c=1\ kA/cm^2$ and $4.5\ kA/cm^2$ were arranged on $5\times5\ mm^2$ chips referenced according to wafer number and the coordinates (in units of 5 mm) of the chip location on the wafer. For example, a chip from wafer KL1004 with location (−5,7) is to be called KL1004N5P7.

III. EXPERIMENT

Each chip was mounted inside a magnetically shielded cryoprobe. The junctions were measured using a low-pass-filtered four-probe setup with a Keithley 2000 voltmeter and a Keithley 6220 current source. Electrical stress was applied at room temperature by ramping current through the junction up to a preselected value I_S at an average rate of 1.4 mA/s and immediately back down to zero at the same rate. The effect of the current ramp rate was not investigated. The stress application was preceded and followed by a measure-

TABLE I. Summary of initial resistances, initial critical current, and breakdown stress current for the samples shown in Fig. 1

Junction	Target J_c (kA/cm^2)	Stress polarity	I_{SB} (mA)	R_0 at 300 K (Ω)	R_{n0} at 4.2 K (Ω)	I_{c0} at 4.2 K (μA)
KL1004N5N6	1.0	+	56	9.27	7.22	180
KL1007N5N6	1.0	–	32	7.88	6.21	177
KL1023P5P7	4.5	+	40	13.3	10.8	118
KL1023P5N8	4.5	–	20	13.4	10.7	120

ment of the junction's room temperature resistance, using a low current of 500 μA. The tunneling *I-V* characteristics were then measured in the superconducting state at $T=4.2$ K with the cryoprobe submerged in liquid He. The next stress/measurement cycles were then performed using progressively higher values of I_S.

The effect of stress polarity was also investigated. Here we define positive stress as current flowing from the counterelectrode (positive potential on the top Nb layer) to the base electrode (Nb/Al bilayer), while negative stress is current flowing in the opposite direction. At room temperature, there is a resistance in series with the tunnel barrier associated with the normal resistance of interconnects to the junction. This series resistance was estimated from the interconnects' geometry using a separately measured sheet resistance of the layers involved. This resistance was assumed to remain unchanged by stress applications and was simply subtracted from the total measured resistance, thus allowing us to estimate the potential difference that develops across the tunnel barrier during stressing. Parameters of some of the studied junctions are given in Table I.

IV. EXPERIMENTAL RESULTS

Figure 1 shows the resistance at low currents (<500 μA) of four Nb/Al/AlO_x/Nb junctions after each subsequent stress application. The junction resistance remains roughly constant after stressing with low currents until a threshold stress current for breakdown I_{SB} is reached, above which the resistance starts to decrease indicating irreversible changes in the barrier. Each succeeding decrease in resistance is apparently a cumulative effect of all previous stress applications. The threshold current varies among nominally identical junctions on the wafer and from wafer to wafer, suggesting some statistical nature of the barrier breakdown. Despite these variations, the observed threshold current for the positive stress (current from Nb counterelectrode to Al) is consistently higher than for negative stress as listed in Table I. If the resistance after stressing is scaled with the resistance R_0 of the initial junction and the stress current is scaled with the threshold current I_{SB}, all the curves in Fig. 1 collapse onto a single curve (see Fig. 1, inset) suggesting a universal breakdown mechanism and a universal character of resistance changes due to electrical stress.

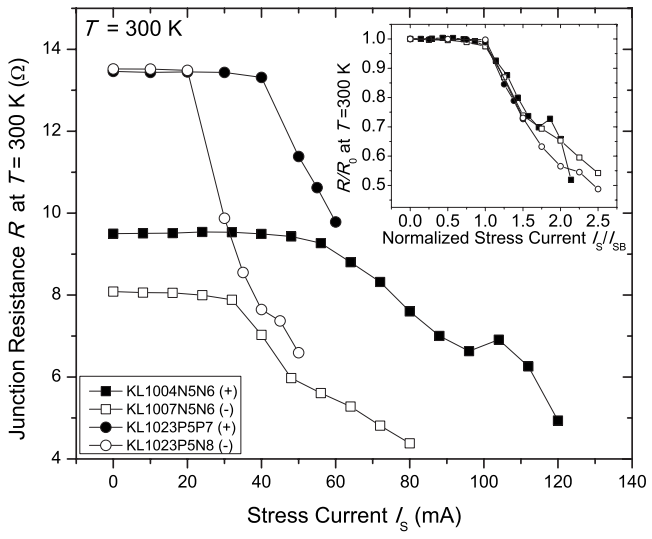

FIG. 1. Junction resistance at room temperature after electrical stressing of the junctions in Table I; (+)/(–) indicates positive/negative stress polarity. Despite small differences between individual junctions, the stress-induced irreversible resistance changes are very similar as demonstrated in the inset showing the normalized resistance R/R_0 at room temperature as a function of normalized stress current I_S/I_{SB} for the same junctions (see Table I).

The irreversible decrease of the tunnel barrier resistance may be due to (a) a decrease in the average barrier height and/or thickness; (b) the barrier becoming nonuniform due to formation of additional conduction channels (regions with increased barrier transparency which are often called micro- or nanoshorts); and (c) a combination of the above. However, room temperature measurements alone are insufficient to distinguish between these possibilities and measurements in the superconducting state of the junction electrodes are needed.

The electric stress-induced changes in the tunnel barrier properties are clearly seen in the Josephson *I-V* characteristics at $T=4.2$ K shown in Fig. 2(a). Five main features are worth mentioning. First, the Josephson critical current, I_c (defined here as the switching current) increases with the stress current. Second, the normal-state resistance, R_n of the junction decreases with the stress current. Third, the so-called knee structure in the quasiparticle tunneling just above the gap voltage of the junction also shifts to higher currents as the stress increases. Fourth, the junction conductance in the subgap region of voltages increases with the stress current. The retrapping current also increases with the increase in subgap conductance. Finally, the gap voltage V_g is nearly independent of the stress current and decreases only slightly at very high stress currents. The increase in the subgap conductance is by far the most pronounced change in the *I-V* curves of the stressed junctions. For instance, after applying a stress current of 96 mA, the Josephson critical current of the junction increases by a factor of ~2.5 whereas the subgap conductance at 2 mV increases by a factor of ~25.

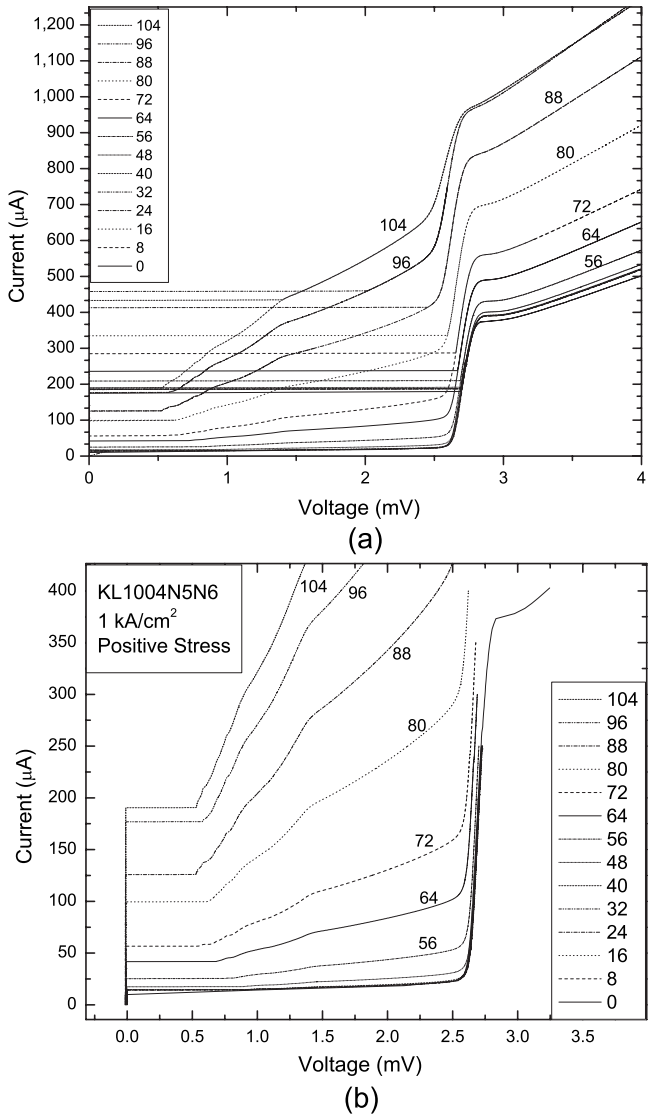

FIG. 2. (a) I-V characteristics of $Nb/Al/AlO_x/Nb$ junction at $T=4.2$ K (initial $J_c=1$ kA/cm^2) after each application of electrical stress shows increasing I_c, decreasing R_n, increasing subgap conductance, and increasing excess current. The gap voltage $V_g=2\Delta/e$ and the current step at $V=V_g$ remain almost unaffected by electric stress in the wide range of stress currents from 0 up to $\sim 2I_{SB}$. At higher stress currents the gap structure broadens and diminishes, and at $I_S \sim 3I_{SB}$ the junction loses all remaining signatures of the tunnel junction. Numbers in the legend indicate the applied positive stress current in milliamperes and identify the curves from top to bottom. (b) Blow up of the return branches of I-V curves of KL1004N5N6 after each stress application clearly shows the development of current steps (subgap structure) at subharmonics of the gap voltage.

V. DISCUSSION

The experimental results presented in Sec. IV show that there is a broad range of electric stress currents through $Nb/Al/AlO_x/Nb$ junctions (and corresponding voltages across the AlO_x tunnel barrier) where a gradual change in the barrier properties occurs. This can be interpreted as a soft breakdown of the oxide barrier in contrast to the sudden changes (hard breakdown) usually observed in thicker oxide layers of SiO_2 and AlO_x. For the junctions with $J_c=1$ kA/cm^2, this range spans from the typical threshold current $I_{SB} \sim 30$ mA (corresponding to a stress current density $J_S \sim 2.4\times 10^5$ A/cm^2) to $I_S \sim 120$ mA ($J_S \sim 10^6$ A/cm^2) above which the stressed devices lose all the signatures of STJs. For the positive stress polarity, the threshold current in Table I, $I_{SB}=56$ mA corresponds to the voltage across the barrier $V_b^+=0.52$ V. For the negative stress polarity, $I_{SB}=32$ mA corresponds to $V_b^-=0.25$ V. The typical barrier thickness d for the Josephson current densities used in this work is ~ 1 nm or less.[25,26] Hence, the typical electric fields across the AlO_x barrier at which the irreversible changes start are $E_b^- \approx 2.5\times 10^8$ V/m and $E_b^+ \approx 5.2\times 10^8$ V/m for the negative and positive stress polarities, respectively.

The difference between V_b^+ and V_b^- was also observed in AlO_x breakdown measurements in MTJs,[8,9] where it was speculated to be a result of different surface roughnesses of the two metal/oxide interfaces. We suggest that the difference between V_b^+ and V_b^- is more fundamental and is a result of difference in work functions of the junction electrodes. Indeed, from the contact potential difference measurements, the work functions in the electrodes are $\varphi_{Al}=4.19$ eV and $\varphi_{Nb}=4.37$ eV for Al and Nb, respectively. Therefore, in a $Nb/Al/AlO_x/Nb$ junction the potential barrier becomes asymmetric and there is an internal electric field across the barrier $E_{int}=\Delta\varphi_{Nb/Al}/ed \sim 1.8\times 10^8$ V/m directed from the Nb/Al base electrode toward the Nb counterelectrode and arising from the difference in work function $\Delta\varphi_{Nb/Al}=\varphi_{Nb}-\varphi_{Al}=0.18$ eV. This barrier asymmetry agrees well with the result obtained from the asymmetry of conductance vs. voltage characteristics of $Nb/Al/AlO_x/Nb$ junctions with low tunnel barrier transparency.[25,26] For the negative stress polarity (lower potential on Nb counterelectrode), the external field adds up to the internal field $E_t^-=E_{ext}+E_{int}$ in the same direction, whereas for the positive stress polarity the external field is opposite to the internal one $E_t^+=E_{ext}-E_{int}$, where E_t is the total field in the dielectric and E_{ext} is the externally applied electric field. If defects in the barrier start to form when the net internal field reaches some critical level E_c (e.g., as a result of ion electromigration), then from the onset of irreversible resistance changes the critical voltage is $V_c=(V_b^+ + V_b^-)/2=0.39$ V, corresponding to $E_c \approx 3.9\times 10^8$ V/m. The barrier asymmetry in this model corresponds to $(V_b^+ - V_b^-)/2 = 0.13$ V, in excellent agreement with the 0.18 V difference between work functions.

Let us see what can be inferred about the nature of stress-induced changes to the barrier from the data presented in Sec. IV. Clearly the increase in the critical current and decrease in the normal resistance of stressed junctions indicate that the critical current density and the average barrier transmission increase. The question is whether the tunnel barrier remains uniform or not. If the barrier remains uniform and only its height and/or thickness is changing with the applied stress, one would expect the junction I_cR_n product to remain constant because in the limit of low barrier transmission probability, it is given by the Ambegaokar–Baratoff (AB) relationship $I_cR_n=\pi\Delta/2e$ for $T \ll T_c$,[27] and the gap voltage was found to remain nearly constant after barrier stressing. Contrary to this, the measured I_cR_n product increases significantly in the stressed junctions as can be seen in Fig. 3. This may indicate a transition from tunnel junction to point contact behavior because for point contacts between two superconductors at $T \ll T_c$ the I_cR_n product is greater

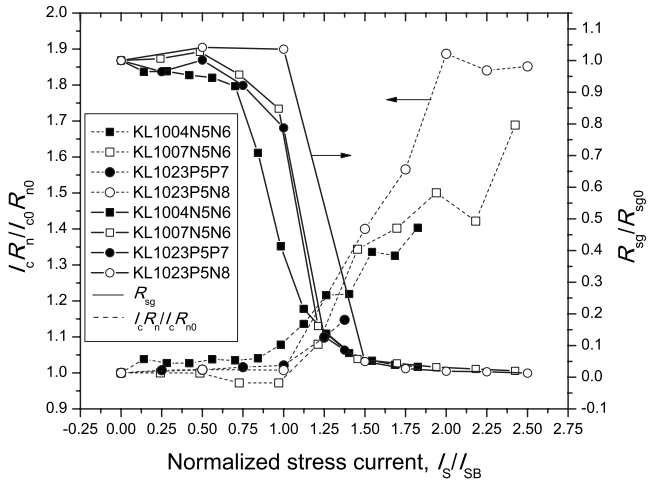

FIG. 3. I_cR_n product (left scale, dotted lines) and R_{sg} at 2 mV (right scale, solid lines) values after each stress application, normalized to their initial values $I_{c0}R_{n0}$ and R_{sg0} in the unstressed junctions. Parameters of the junctions are given in Table I.

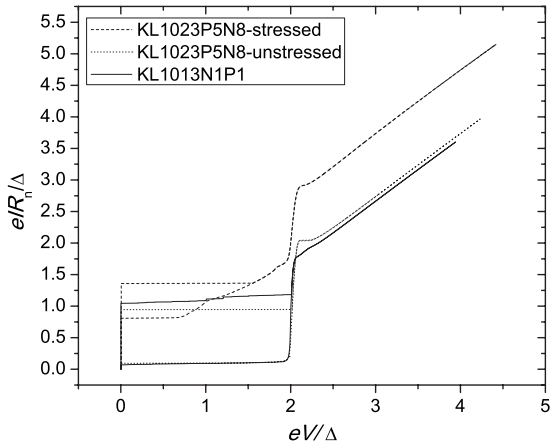

FIG. 4. A comparison of the *I-V* curve of a stressed junction KL1023N5P8 (top dashed curve) with poststress Josephson critical current density $J_c \approx 9$ kA/cm^2 (initial J_c=4.5 kA/cm^2) and an as-fabricated, unstressed junction KL1013N1P1 (solid curve) with $J_c \approx 11$ kA/cm^2. Although the as-fabricated junction has an even larger J_c (larger average barrier transparency), its *I-V* curve is very different from the electrically stressed junction: it has no appreciable subgap conductance, no subharmonic current steps, and no excess current; its I_cR_n product and the current step at V_g are close to the values given by the microscopic theory for tunnel junctions with low transparency. Presumably, the as-fabricated junctions have a uniform tunnel barrier whereas the barrier in electrically stressed junctions becomes nonuniform. The *I-V* curve of the initial, unstressed junction KL1023N5P8 is also shown (dotted curve).

than in the tunnel junction by a factor of 1.32 in the dirty limit and by a factor of 2 in the clean limit, as was shown by Kulik and Omel'yanchuk (KO).[28,29] It was also found by Arnold[30,31] that, for an insulating and structureless barrier of arbitrary thickness, the I_cR_n product in general depends on the barrier transmission probability D, and reduces to the AB result at $D \ll 1$ and to the KO result for the clean point contact at $D=1$.

It is easy to show, however, that the barrier does not remain uniform and structureless after stressing. For this, we compare the *I-V* curves of a stressed junction and an as-prepared, unstressed junction with the same average Josephson critical current density. The as-prepared junction is presumably as uniform as possible for the given fabrication method. The *I-V* curves are shown in Fig. 4. The stressed junction with $J_c \approx 9.3$ kA/cm^2 clearly has different *I-V* characteristics (especially at $V < V_g$) than the as-prepared junction with an even higher $J_c \approx 11$ kA/cm^2. This comparison indicates that the changes in the *I-V* curves and the increase in the I_cR_n product brought about by electric stress cannot be explained by a gradual increase in transparency of a uniform and structureless barrier. A dramatic increase in the subgap conduction in the stressed junctions, the appearance of pronounced features at subharmonics of the gap voltage, $2\Delta/en$ at $n=2,3,\ldots$ shown in Fig. 5 along with the increase in I_cR_n strongly indicate that additional conduction channels with increased transparency are gradually formed as a result of electric stress. These conduction channels can be viewed as point contacts between the junction electrodes, pinholes, or nanoshorts in the barrier, contributing to both the quasiparticle and the Cooper-pair transport in parallel to the main tunnel barrier which remains largely unmodified by the stress.

Subgap features similar to those appearing in electrically stressed junctions [Fig. 2(b) and Fig. 5] have long been observed in Nb/Al/AlO$_x$/Nb and other types of junctions[13–15] with high critical current densities and attributed to multiple Andreev reflections (MARs). Two models were proposed to explain the appearance of MAR steps in high-J_c junctions. Kleinsasser *et al.*[32] suggested that as oxygen exposure during Al oxidation decreases, the barrier becomes nonuniform, consisting of regions with low transparency (good tunnel barrier) and regions with high transparency (pinholes). That is, the transparency distribution has two sharp peaks, one at a low D value and another one at $D \sim 1$. As oxygen exposure decreases, the relative contribution of the second peak increases, and so does the J_c. Naveh *et al.*[33] argued that the defects in the ultrathin tunnel barrier are naturally occurring and, therefore, the transparency distribution in high-J_c junctions is universal and given by the Schep–Bauer (SB) distribution[33]

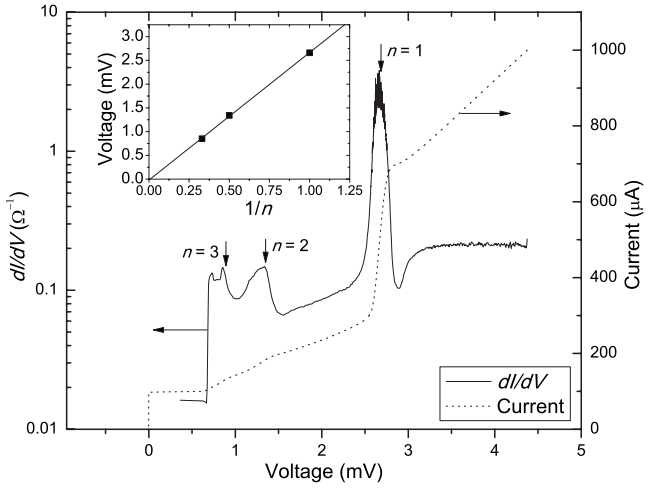

FIG. 5. The return branch of the *I-V* characteristic (dotted curve) of KL1004N5N6 after application of 80 mA stress along with differential conductance dI/dV (solid curve) showing peaks corresponding to MARs of quasiparticles. The inset shows the voltages corresponding to conductance peaks; the straight line is a fit to $2\Delta/en$ ($n=1,2,\ldots$) dependence expected for MARs, giving $2\Delta/e=2.696$ mV.

$$\rho(D) = \frac{G}{\pi G_0} \frac{1}{D^{3/2}\sqrt{1-D}}. \quad (1)$$

They found that SB distribution gives a better fit to experimental *I-V* curves than averaging over the Dorokhov distribution describing the transparency distribution in long disordered conductors—not a surprise though because the Dorokhov distribution should not be applicable to short channels by definition. There is ample experimental evidence however that the behavior of high-J_c junctions is not universal. For instance, the value of J_c at which MAR steps become visible strongly depends on the junction fabrication procedure and varies between different experimental groups.[14,15] Our experimental results show that MAR steps can be created at will in tunnel barriers with any initial transparency as a result of electrical stress. Therefore, what were perceived as natural and universal defects appearing in the oxide barrier as a result of a short oxidation process[34] could be simply a result of damage to the very thin tunnel barrier induced during the junction (wafer) fabrication processes. This could explain why improvements in the junction fabrication process usually shift the J_c level at which MAR steps begin to appear toward higher values.

Although no microstructural characterization of the barrier changes was undertaken in this work, a plausible scenario of how the additional conduction channels are induced by electric stress can be proposed. It is known that AlO_x formed by room temperature oxidation is amorphous and nonstoichiometric, i.e., contains a large amount of oxygen vacancies.[35] At the oxidation conditions used in our work, the barrier thickness is only ~1 nm, i.e., just about two to three nearest-neighbor distances. Therefore, a displacement of even a single atom from the barrier can significantly increase local transparency. If a dc electric field is applied to the oxide barrier, electromigration of cations (Al^{3+}) and anions (O^{2-},O^{-}) in opposite directions may occur. From anodic oxidation of Al in electrolytes it is known that the anodizing ratio for Al is ar=1.3 nm/V, i.e., 1.3 nm of AlO_x is formed for each volt applied to the Al/electrolyte interface.[36] That is, on average, oxygen ions are transported inside the aluminum electrode by ~1 nm per 1 V of applied voltage. Ionic current density in the oxide is a strong function of the electric field strength $J_i = \alpha \exp(\beta E - \gamma E^2)$.[36,37] In our case, there is no electrolyte providing a constant supply of oxygen atoms for the oxide to grow. However, some oxygen ions from AlO_x barrier will electromigrate into Al underlayer of the Nb/Al/AlO_x structure if the Nb/Al base electrode is at a positive potential (negative stress polarity in our nomenclature) while Al^{3+} cations should migrate toward the interface with Nb counterelectrode. At a positive potential on Nb counterelectrode (positive stress), oxygen ions from the AlO_x barrier will move into Nb counterelectrode, depleting the barrier. The average oxygen displacement at the onset of breakdown can be estimated using the typical threshold voltage $V_b^- = 0.25$ V and ar=1.3 nm/V, giving ~0.3 nm. This closely corresponds with O–O nearest-neighbor distance of 2.8 Å in amorphous alumina.[38]

Any ion displacement in the barrier under the effect of an applied electric field creates a defect and alters the barrier transparency. The length of the newly created conduction channel is about the same as the barrier thickness which is much less than the coherence length ξ and the magnetic field penetration depth λ. The cross section of such a channel is also on the atomic scale, much less than ξ and λ. The theory of current transport through such short and narrow channels, often called quantum point contacts (QPCs), is well developed. For the single mode QPC, the Josephson current is given by

$$I = \frac{e\Delta}{2\hbar} \frac{D \sin\phi}{\sqrt{1 - D\sin^2(\phi/2)}} \tanh \frac{\Delta\sqrt{1 - D\sin^2(\phi/2)}}{k_B T}, \quad (2)$$

where D is the channel transparency and ϕ is the phase difference.[39]

The theory of nonstationary properties in superconducting QPCs (SQPCs) was developed by Averin and Bardas.[40] It is based on the idea of MARs (Ref. 41) which reveal themselves as current steps at subharmonics of the gap voltage $2\Delta/en$, at $n=2,3,\ldots$. They found that *I-V* characteristics strongly depend on the SQPC transparency and demonstrate the most pronounced subharmonic steps at intermediate values of $D \sim 0.4$ to 0.5. The theoretical *I-V* curves reduce to a pure tunneling characteristics at $D < 0.1$ and to a featureless curve typical for an *I-V* of a clean S–N interface at $D \sim 1$ (Ref. 40) (see Fig. 6).

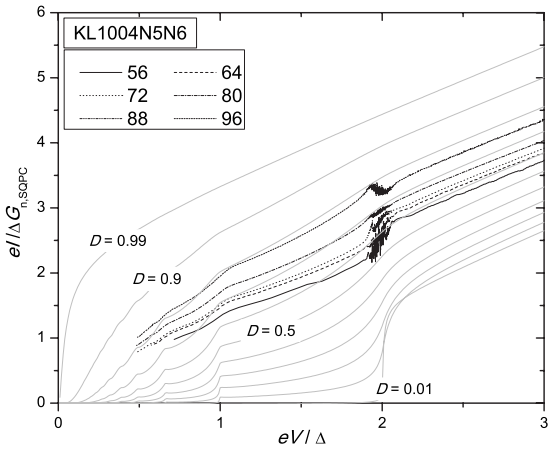

FIG. 6. Normalized *I-V* characteristics of the additional conduction channels (SQPCs) created by positive electric stressing at currents $I_S = 56, 64, \ldots, 96$ mA. The curves were obtained by subtracting the *I-V* characteristics of the initial, unstressed junction $I_0(V)$ from the *I-V* curve after each stress application, $I_{SQPC}(V) = I(V) - I_0(V)$. The dip at $eV/\Delta = 2$ in the curves is an artifact of the subtraction procedure due to some broadening and slight decrease in the gap after electric stressing. Theoretical *I-V* curves for a single SQPC with varying transparency $D = 0.01, 0.1, 0.2, 0.3, \ldots, 0.8, 0.9, 0.99$ (bottom to top) from Ref. 40 are also shown. As can be seen, all the obtained experimental dependences fall within the range of theoretical curves corresponding to $0.6 \lesssim D \lesssim 0.8$.

Let us see what properties of conduction channels created in the AlO_x barrier by electrical stressing can be inferred from the measured *I-V* curves shown in Fig. 2. Because of space constraints we will restrict our analysis to the positive stress polarity only. The case of the negative stress polarity is completely analogous and will be presented elsewhere. First, we note that the amplitude of the current step ΔI_{ss} at $V_g = 2\Delta/e$ practically does not change in stressed junctions although the subgap conductance dramatically increases. (In

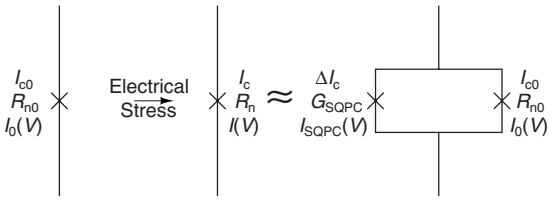

FIG. 7. Circuit diagram of the proposed model. In this model, the application of electrical stress results in the formation of few additional conduction channels G_{SQPC} in the tunnel barrier which remains largely unchanged and is assumed to be the same as the initial, unstressed junction.

the first approximation we will neglect some broadening of the current step at V_g and a small decrease in V_g at extremely high stress currents which could result from the smearing of the metal-insulator interfaces.) In the microscopic theory of tunneling in superconductors, the size of the current step is proportional to the area of the tunnel barrier and is given by

$$\Delta I_{ss} = G_{NN} A \frac{\pi \Delta}{2e}, \tag{3}$$

where G_{NN} is the specific normal-state tunneling conductance.

It is easy to verify that the experimentally observed ΔI_{ss} in Fig. 2 is very close to the value given by Eq. (3). The independence of ΔI_{ss} of electric stress indicates that the area of the tunnel barrier and its conductance does not change noticeably. It means that the total area of additional conduction channels formed by stressing is much smaller than the junction area. Therefore, a stressed junction can, in the first approximation, be represented by a parallel combination of the initial (unstressed) junction and some number of SQPCs (see Fig. 7): $I(V)=I_0(V)+I_{SQPC}(V)$. To obtain the *I-V* characteristics of these SQPCs, $I_{SQPC}(V)$, we can subtract the *I-V* curve of the tunnel (unstressed) junction $I_0(V)$ from the experimental $I(V)$ in the stressed junction. The result of this procedure is shown in Fig. 6, along with the theoretical *I-V* curves calculated for a SQPC with different transparencies.[40]

Although the subtraction procedure is not very accurate near the gap voltage because of the gap smearing in the highly stressed junction, it is clear that the *I-V* curve of the SQPCs has no significant current step at $V=2\Delta/e$. This is true for any stress current I_S (any number of SQPCs) because in all the *I-V* curves in Fig. 2 the current step at $V=2\Delta/e$ is the same as in the initial junction. In the microscopic theory of nonstationary properties of a single SQPC,[40] the size and broadening of the current step at $V=2\Delta/e$ in the *I-V* curve as well as the size and broadening of subharmonic current steps strongly depends on the channel transparency. The step at $2\Delta/e$ basically disappears at $D>0.6$ while subharmonic steps basically disappear at $D>0.9$. Therefore, in the theory, the range of channel transparencies where the *I-V* curves would look like in Figs. 2(b) and 6 is very narrow $0.6 \lesssim D \lesssim 0.8$. Hence, it would not make a significant error if, for simplicity, we assume that all the channels have the same transparency. A better approach would only be a full fitting of the *I-V* curves to the theory, which will be done elsewhere. It can be seen from Fig. 6 that all the *I-V* curves of SQPCs formed in the stress current range from the breakdown I_{SB} to $2I_{SB}$ lie between the theoretical curves with $D=0.6$ and $D=0.8$. Therefore, the average channel transparency formed at electric stressing can be taken as $\langle D \rangle = 0.7$.

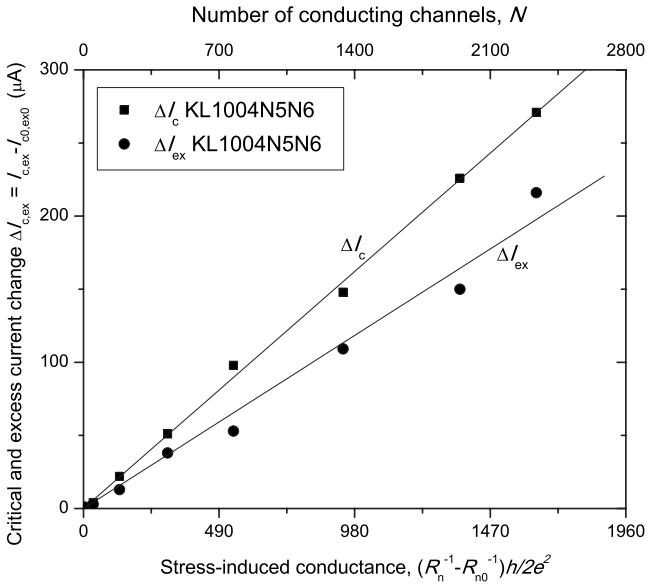

FIG. 8. The change in critical current and excess current caused by electric stressing as a function of the change in the normal-state conductance (bottom scale) and the number of created channels (top scale) based on $\langle D \rangle = 0.7$. The straight line is the linear fit giving the average I_c per channel of 0.115 μA and $\delta I_{ex}=0.084$ μA/channel.

From the linear part of the *I-V* curves at $V>V_g$, the normal-state conductance of the channels is simply $G_{SQPC}=R_n^{-1}-R_{n0}^{-1}$, where R_{n0} is the normal-state tunnel resistance of the initial junction measured before stressing. Since the normal-state conductance of a single QPC is given by $2e^2D/h$, we can estimate the number N of created SQPCs using $N\cdot\langle D \rangle = G_{SQPC}h/2e^2$. At $\langle D \rangle = 0.7$, the number of channels formed at the maximum stress currents studied is $\sim 2\times 10^3$, corresponding to an average channel density of 1.6×10^{10} channels/cm^2 and an average channel spacing of ~80 nm. In our model each channel is associated with a displaced ion in the barrier, so the estimates above give the surface density and the average distance between displaced ions in the barrier at the maximum stress current $I_S=104$ mA. The obtained estimates are self-consistent with the initial supposition that the number of additional conduction channels is small and that the area occupied by the channels is negligible with respect to the area of the tunnel barrier.

Since each SQPC carries a supercurrent, the increase of the critical current in the stressed junctions $\Delta I_c = I_c - I_{c0}$ should be proportional to the number of conducting channels. This is shown in Fig. 8. Using the assumption of equal channel transparency and $\langle D \rangle \sim 0.7$, we can estimate the average contribution of each created channel $\delta I_c = \Delta I_c/N$ from Fig. 8 to be about 0.115 μA/channel. Using the experimental value of $\Delta/e=1.35$ mV and $\langle D \rangle = 0.7$, from Eq. (2) we obtain the theoretical value of $\delta I_c = 0.147$ μA/channel, a very close value.

The theory[40] also explains the existence of the excess current in the *I-V* curves as a nonzero average of the Joseph-

son ac current at finite voltages. It can be seen in Fig. 6 that the part of experimental *I-V* curves at $V > V_g$ (region of the excess current) agrees very well with the theory. The excess current defined as $\Delta I_{ex} = I_{ex} - I_{ex0}$ is shown in Fig. 8, where I_{ex} was determined by fitting the *I-V* curves at $V > V_g$ to $I(V) = I_{ex} + V/R_n$ and index 0 identifies the initial, unstressed junction. The straight line fit yields $\delta I_{ex} = 0.084$ μA/channel, or $\delta I_{ex}/\delta I_c = 0.73$ in very good agreement with the theory,[40] giving $\delta I_{ex}/\delta I_c = 2/\pi$ at $D \sim 1$.

So, by analyzing the additional subgap conductance, additional normal-state conductance, and additional Josephson currents induced by electric stressing of the junction's barrier we obtained a self-consistent picture. In this picture, after a point of soft breakdown has been reached, atomic-size conduction channels with similar transparencies are being formed in the barrier as the stressing progresses. We also proposed a scenario in which the formation of these channels is a result of electric-field-stimulated ion migration away from the barrier. Let us see if this scenario also agrees with the available experimental data.

The treatment of ion transport in an electric field (electromigration) is very well known and goes back to the original Frenkel defect theory and works by Mott,[42] and Cabrera and Mott.[43] Following Ref. 43 the ionic current density can be written as

$$J_i = 2an\nu q[e^{-(W-qaE)/k_BT} - e^{-(W+qaE)/k_BT}] = an\nu e^{-W/k_BT} \sinh(qaE/k_BT), \quad (4)$$

where n is the concentration of the mobile ions, ν is the attempt frequency, W is the activation energy, q is the ion charge, and a is the activation or half-jump distance. Ionic (atomic) transport in solids usually proceeds via vacancy exchange mechanism (in which case W is the height of the energy barrier the ion needs to overcome) or via formation of Frenkel defects (vacancy-interstitial pairs), in which case W is the activation energy for formation of a Frenkel defect. The total number of displaced ions in the barrier can be hence presented as

$$N = Bt \sinh(qAE/k_BT) = Bt \sinh(V/V_0), \quad (5)$$

where t is the stress duration, V is the voltage across the barrier, $V_0 = k_BTd/qa$, d is the barrier thickness, and B is a temperature-dependent parameter.

Since in our model each displaced ion represents a new conduction channel, in Fig. 9 we plotted the "effective" number of conduction channels determined from the increase in the junction conductance $N \cdot \langle D \rangle = G_{SQPC}h/2e^2$ as a function of maximum voltage across the junction which develops during each stressing at room temperature. The dependence given by Eq. (5) is also shown and fits the data very well, giving $V_0 = 0.045 \pm 0.005$ V. Assuming that oxygen ions are the mobile species, we can take $q = 2e$, $a = 2.8$ Å (nearest-neighbor distance), $d = 1$ nm, and $T = 300$ K, and get from Eq. (5) $V_0 = 0.046$ V in excellent agreement with the experimental data in Fig. 9. If instead we use the value $qa = 4.28$ e Å determined from direct measurements of ionic current in alumina films,[37] the fit to the experimental data in Fig. 9 gives a tunnel barrier thickness $d = 0.76$ nm which is in a better agreement with the barrier thickness data[25,26] obtained from differential conductance versus voltage dependences.

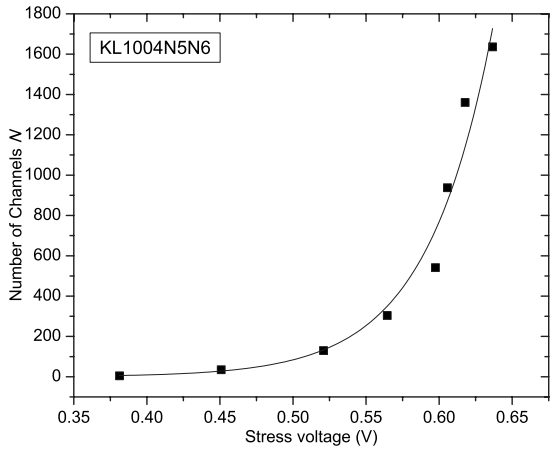

FIG. 9. The number of created channels N (assuming $\langle D \rangle = 0.7$) vs the maximum applied stress voltage. The solid curve is the fit to Eq. (5) yielding $V_0 = 0.045$ V. This is very close to the calculated value of $V_0 = 0.046$ V.

A secondary objective of this research was to relate the above studied effect of dc electrical stress with anomalous *I-V* characteristics of Josephson junction arrays frequently observed for many fabrication processes.[20,21,44] As was described in Sec. I, usually one or two junctions at the ends of the array demonstrate an I_c that is significantly larger than the average I_c of the other junctions in the array, see Fig. 10. Usually, the junction with the highest deviation from the average is the last junction in the array, the one which has the base electrode directly connected to the ground plane layer.[20,21] The second deviating junction is the first junctions in the array, the one which is connected by the wiring layer to the chip contact pads.[20] These usually large deviations in I_c are also reflected in the so-called knee region of the *I-V*

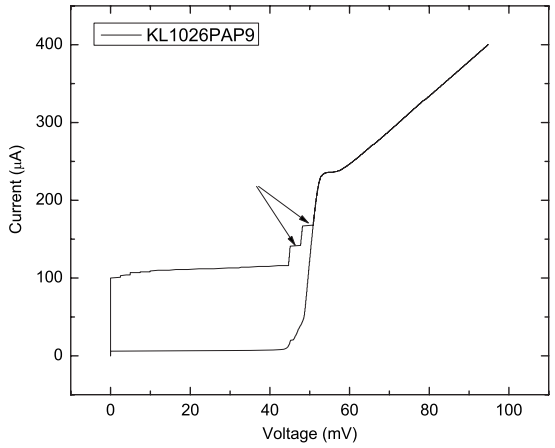

FIG. 10. *I-V* curve of an as-fabricated 20-junction series array. Two junctions with significantly higher I_c than the rest of the array are shown by arrows. Whereas the characteristics of these two junctions are qualitatively similar to those of the electrically stressed junctions in this study, the amount of electric current that is required to damage the stressed junctions [$I_{SB} \times$ (number of junctions)] cannot be supplied by the plasma processes employed during the fabrication. Hence, this fabrication-induced variation in I_c in this array is unlikely to be caused by electron current-induced breakdown of the tunnel barriers.

curve where the knee current of the junctions in question is much higher and can be distinctly seen in the normal branch of the curve. Furthermore the subgap conductance corresponding to these two junctions is significantly higher than the average. MAR steps in the subgap region of these junctions have also been observed.[21]

Qualitatively, these anomalous junctions look like the junctions subjected to electric stress as described above. Electric currents can flow through some of the Josephson junctions during their fabrication, e.g., during reactive ion etching. The question is whether the amplitude of the current is high enough to cause degradation of the barrier in many junctions on the wafer. From the results of dc electric stressing, we have found that the typical breakdown current in the smallest junctions used in superconductor integrated circuits is $I_{SB} \sim 32$ mA, at which a critical voltage develops across the barrier, i.e., $I_{SB}/I_c \sim 250$. The typical 0.25 cm^2 test chip contains ~20 Josephson junction arrays. Therefore, to cause breakdown of all 20 grounded junctions in these arrays, it would need a current density of ~2.6 A/cm^2 because for plasma-induced current the grounded junctions are all connected in parallel. There are also several test chips spread out on the 150 mm wafers so the total current through the wafer should be huge. The typical rf power used for etching in our process is from 40 to 150 W and peak-to-peak voltage is from 305 to 900 V depending on the circuit layer, corresponding to power density from 88 to 332 mW/cm^2. Although, rf power is coupled capacitively to the wafer and to the circuits' ground plane, the rf current can flow directly through the junctions which are galvanically coupled to the ground plane. Estimating the amplitude of electric current supplied by the rf source, we find it to be in the range of 0.5–0.7 A, corresponding to the current density from 1 to 1.55 mA/cm^2. This is clearly too small a current to cause significant damage to oxide barriers in Josephson junctions. Therefore, we conclude that although exposure to processing plasma has a potential in creating voltage differences on the wafer surface which are large in comparison with the typical breakdown voltages in ultrathin oxide barriers,[45] the typical etching plasmas used in superconductor integrated circuits fabrication do not supply enough current to electrically break down the tunnel barriers of Josephson junctions due to their high tunneling conductance. The same conclusion was also reached in Ref. 21.

Because of these results, it is likely that the damage to junctions galvanically coupled to the ground plane or other circuit layers observed in Ref. 20 is chemical or electrochemical in nature. For instance, it can be due to diffusion or electromigration of impurity atoms from the layers in direct contact with the junction to the junction's electrodes and to the barrier, e.g., hydrogen atoms dissolved in Nb. In many respects the features of oxide barrier damage by H^+ electromigration should be similar to that of electron current damage. However, the required currents can be substantially lower because hydrogen is known to be highly mobile in Nb. Therefore, it should be much easier to cause diffusion of hydrogen atoms in Nb toward the barrier than to displace oxygen atoms from the AlO_x oxide barrier. This damage mechanism will be considered separately.

VI. CONCLUSION

We have studied the effect of dc electric stress (current) applied at room temperature to $Nb/Al/AlO_x/Nb$ junctions with $J_c = 1.0$ and 4.5 kA/cm^2 on their Josephson and quasiparticle tunneling properties. We have observed a very soft breakdown: above a certain threshold stress current I_{SB} the changes in *I-V* characteristics indicate formation in the barrier of additional conduction channels with increased transparency. These channels reveal themselves in the dramatic increase in the subgap conduction, the appearance of subharmonic current steps (MARs), an increase in the critical current, a decrease in the normal-state resistance, and an increase in the I_cR_n product. The range of the stress currents over which these gradual changes occur is quite broad, from I_{SB} to $\gtrsim 2I_{SB}$, corresponding to $\sim 250I_c$ to $\gtrsim 500I_c$. The threshold (breakdown) current depends on the stress current polarity and is larger when the Nb counterelectrode is at a positive potential.

We have suggested that the soft breakdown proceeds via formation of defects in the barrier as a result of ion migration in the applied electric field. The stress polarity dependence was explained as due to internal electric field caused by the difference in the work functions of the junction electrodes. The observed breakdown fields $E_c \sim 3.9 \times 10^8$ V/m ($V_c \cong 0.39$ V across the barrier) correspond to the magnitude required for near-neighbor displacement of oxygen ions.

From the changes in the tunneling characteristics in the superconducting state we concluded that the total area of the additional conduction channels is much smaller than the area of the initial tunnel barrier, and that they can be considered as connected in parallel to the initial tunnel junction whose properties remain virtually unchanged by electric stressing. Using this parallel connection model, we estimated the transparency of the additional conduction channels by comparing their *I-V* characteristics to the nonstationary theory of current transport in SQPCs by Averin and Bardas. We found that all the channels have similar transparencies D in the range from ~0.6 to ~0.8. We found an excellent agreement of the shape of *I-V* characteristics of the conduction channels created by electric stressing with the Averin–Bardas[40] theory for SQPCs. From the change in the normal-state resistance we calculated the effective number of the additional conduction channels N. The observed changes in the junction critical current per channel and the excess current per channel were found to be consistent with the predictions of the microscopic theory for SQPCs.

We also found an exponential dependence of the number of additional conduction channels created by electric stressing on the stress voltage, $N \sim \sinh(V/V_0)$. The characteristic voltage V_0 was found to be in excellent agreement with the proposed model of defect formation by ion electromigration out of the barrier.

Due to the high tunneling conductance of oxide barriers used in superconductor digital electronics it is unlikely that breakdown currents can be reached during plasma processing steps of junction fabrication. However, it is possible that electromigration and diffusion of impurity atoms in Nb lay-

ers is responsible for pattern-dependent tunnel barrier degradation frequently observed in superconductor integrated circuits.

ACKNOWLEDGMENTS

We would like to thank Daniel Yohannes, Richard Hunt, and John Vivalda for their part in wafer processing. Many discussions with Alex Kirichenko, Timur Filippov, Vasili Semenov, and Dmitri Averin are highly appreciated. We would also like to thank D. Averin for providing the program for calculating the theoretical curves shown in Fig. 6. We are also grateful to Deborah Van Vechten for her interest and support in this research. This work was supported by the ONR Grant Nos. N000140810224 and N000140710093.

[1]R. Degraeve, G. Groeseneken, R. Bellens, J. Ogier, M. Depas, P. Roussel, and H. Maes, IEEE Trans. Electron Devices **45**, 904 (1998).
[2]W. J. Chang, M. P. Houng, and Y. H. Wang, J. Appl. Phys. **89**, 6285 (2001).
[3]M. Alam, B. Weir, and P. Silverman, IEEE Trans. Electron Devices **49**, 232 (2002).
[4]M. Alam, B. Weir, and P. Silverman, IEEE Trans. Electron Devices **49**, 239 (2002).
[5]K. Shimazawa, N. Kasahara, J. J. Sun, S. Araki, H. Morita, and M. Matsuzaki, J. Appl. Phys. **87**, 5194 (2000).
[6]J. Das, R. Degraeve, H. Boeve, P. Duchamps, L. Lagae, G. Groeseneken, G. Borghs, and J. De Boeck, J. Appl. Phys. **89**, 7350 (2001).
[7]B. Oliver, G. Tuttle, Q. He, X. Tang, and J. Nowak, J. Appl. Phys. **95**, 1315 (2004).
[8]K. Kim and B. K. Cho, Appl. Phys. Lett. **86**, 142106 (2005).
[9]J. Akerman, M. DeHerrera, J. Slaughter, R. Dave, J. Sun, J. Martin, and S. Tehrani, IEEE Trans. Magn. **42**, 2661 (2006).
[10]R. M. Hill and L. A. Dissado, J. Phys. C **16**, 2145 (1983).
[11]R. M. Hill and L. A. Dissado, J. Phys. C **16**, 4447 (1983).
[12]J. W. McPherson and H. C. Mogul, J. Appl. Phys. **84**, 1513 (1998).
[13]A. W. Kleinsasser, F. M. Rammo, and M. Bhushan, Appl. Phys. Lett. **62**, 1017 (1993).
[14]R. E. Miller, W. H. Mallison, A. W. Kleinsasser, K. A. Delin, and E. M. Macedo, Appl. Phys. Lett. **63**, 1423 (1993).
[15]V. Patel and J. Lukens, IEEE Trans. Appl. Supercond. **9**, 3247 (1999).
[16]K. K. Likharev and V. K. Semenov, IEEE Trans. Appl. Supercond. **1**, 3 (1991).
[17]I. V. Vernik, D. E. Kirichenko, V. V. Dotsenko, R. Miller, R. J. Webber, P. Shevchenko, A. Talalaevskii, D. Gupta, and O. A. Mukhanov, Supercond. Sci. Technol. **20**, S323 (2007).
[18]S. K. Tolpygo, D. Yohannes, R. T. Hunt, J. A. Vivalda, D. Donnelly, D. Amparo, and A. F. Kirichencko, IEEE Trans. Appl. Supercond. **17**, 946 (2007).
[19]W. Chen, A. V. Rylyakov, V. Patel, J. E. Lukens, and K. K. Likharev, Appl. Phys. Lett. **73**, 2817 (1998).
[20]S. K. Tolpygo, D. Amparo, A. Kirichenko, and D. Yohannes, Supercond. Sci. Technol. **20**, S341 (2007).
[21]S. K. Tolpygo and D. Amparo, J. Phys.: Conf. Ser. **97**, 012227 (2008).
[22]M. Konkin and J. Adler, J. Appl. Phys. **51**, 5450 (1980).
[23]HYPRES Niobium Integrated Circuit Fabrication Design Rules, Hypres, Inc., 2008, http://www.hypres.com/pages/download/designrules/DesignRules.pdf
[24]M. Gurvitch, M. A. Washington, and H. A. Huggins, Appl. Phys. Lett. **42**, 472 (1983).
[25]S. Tolpygo, E. Cimpoiasu, X. Liu, N. Simonian, Y. Polyakov, J. Lukens, and K. Likharev, IEEE Trans. Appl. Supercond. **13**, 99 (2003).
[26]E. Cimpoiasu, S. K. Tolpygo, X. Liu, N. Simonian, J. E. Lukens, K. K. Likharev, R. F. Klie, and Y. Zhu, J. Appl. Phys. **96**, 1088 (2004).
[27]V. Ambegaokar and A. Baratoff, Phys. Rev. Lett. **10**, 486 (1963).
[28]I. O. Kulik and A. N. Omel'yanchuk, Sov. Phys. JETP **21**, 96 (1975).
[29]I. O. Kulik and A. N. Omel'yanchuk, Sov. J. Low Temp. Phys. **4**, 142 (1978).
[30]G. B. Arnold, J. Low Temp. Phys. **59**, 143 (1985).
[31]G. B. Arnold, J. Low Temp. Phys. **68**, 1 (1987).
[32]A. W. Kleinsasser, R. E. Miller, W. H. Mallison, and G. B. Arnold, Phys. Rev. Lett. **72**, 1738 (1994).
[33]Y. Naveh, V. Patel, D. Averin, K. Likharev, and J. Lukens, Phys. Rev. Lett. **85**, 5404 (2000).
[34]W. H. Mallison, R. E. Miller, and A. W. Kleinsasser, IEEE Trans. Appl. Supercond. **5**, 2330 (1995).
[35]E. Tan, P. G. Mather, A. C. Perrella, J. C. Read, and R. A. Buhrman, Phys. Rev. B **71**, 161401(R) (2005).
[36]J. W. Diggle, T. C. Downie, and C. W. Goulding, Chem. Rev. (Washington, D.C.) **69**, 365 (1969).
[37]M. J. Dignam and P. J. Ryan, Can. J. Chem. **46**, 549 (1968).
[38]P. Lamparter and R. Knieper, Physica B (Amsterdam) **234–236**, 405 (1997).
[39]C. Beenakker, Phys. Rev. Lett. **67**, 3836 (1991).
[40]D. Averin and A. Bardas, Phys. Rev. Lett. **75**, 1831 (1995).
[41]A. F. Andreev, Sov. Phys. JETP **19**, 1228 (1964).
[42]N. F. Mott, Trans. Faraday Soc. **43**, 429 (1947).
[43]N. Cabrera and N. F. Mott, Rep. Prog. Phys. **12**, 163 (1949).
[44]M. Hidaka, S. Nagasawa, K. Hinode, and T. Satoh, IEICE Trans. Electron. **E91-C**, 318 (2008).
[45]K. Cheung, *Plasma Charging Damage* (Springer, Berlin, 2000).